Journal of CO2 Utilization 42 (2020) 101352

Contents lists available at ScienceDirect

Journal of CO2 Utilization

journal homepage: www.elsevier.com/locate/jcou

Arc plasma reactor modification for enhancing performance of dry reforming of methane

Duy Khoe Dinh [a,b,1], Georgi Trenchev [c,1], Dae Hoon Lee [a,b,*], Annemie Bogaerts [c,**]

[a] University of Science and Technology (UST), Republic of Korea
[b] Korean Institute of Machinery and Materials, Republic of Korea
[c] University of Antwerp, Research Group PLASMANT, Universiteitsplein 1, B-2610, Antwerp, Belgium

ARTICLE INFO

Keywords:
Rotating arc
Vortex stabilized gliding arc
Arc dynamics
Dry reforming of methane

ABSTRACT

Arc plasma technology is gaining increasing interest for a variety of chemical reaction applications. In this study, we demonstrate how modifying the reactor geometry can significantly enhance the chemical reaction performance. Using dry reforming of methane as a model reaction, we studied different rotating arc reactors (conventional rotating arc reactor and nozzle-type rotating arc reactor) to evaluate the effect of attaching a downstream nozzle. The nozzle structure focuses the heat to a confined reaction volume, resulting in enhanced heat transfer from the arc into gas activation and reduced heat losses to the reactor walls. Compared to the conventional rotating arc reactor, this yields much higher CH_4 and CO_2 conversion (i.e., 74% and 49%, respectively, versus 40% and 28% in the conventional reactor, at 5 kJ/L) as well as energy efficiency (i.e., 53% versus 36%). The different performance in both reactors was explained by both experiments (measurements of temperature and oscillogram of current and voltage) and numerical modelling of the gas flow dynamics, heat transfer and fluid plasma of the reactor chambers. The results provide important insights for design optimization of arc plasma reactors for various chemical reactions.

1. Introduction

Plasma is an ionized gas that contains highly reactive species (i.e., electrons, ions, radicals and excited species), and it has been used for a variety of energy and environmental applications [1–9]. For example, dielectric barrier discharge (DBD) plasma has been widely used for ozone generation [10], while arc plasma has been applied for assisting combustion with lower NO_x emission, increased flame stability, and reduced fuel consumption [11–14]. A thermal plasma torch can provide a higher temperature environment than in a traditional combustion process, which is advantageous for thermal activation of stable chemicals and nanopowder production [15–20].

Chemical activation by plasma is promising to solve emerging issues of the environment and global warming, because of its unique advantages, such as fast start-up, compactness, high density of energetic species, and (for some plasma types) high-temperature condition. Among various plasma types, non-thermal arc plasma, with a typical gas temperature of a few thousand Kelvin, hence much lower than the electron temperature of 1 —2 eV, has been reported as one of the best performing plasma sources for various chemical applications, such as CO_2 conversion, dry reforming of methane (DRM), nitrogen fixation, and methane activation [21–30]. It is induced by high voltage and low current power supplies (current below 10 A and voltage ranging from several to tens of kV, based on the definition of Kalra et al. [31]). The arc contains a high electron density and relatively high gas temperature. The electron temperature in non-thermal arc plasma is approximately 1–2 eV, while the gas temperature is a few thousand Kelvin (2000–4000 K); hence, still much lower than the electron temperature [29,31–33]. Therefore, it is called “non-thermal arc” or “warm plasma”, as well as “high-voltage and low-current arc”, as opposed to thermal arc plasmas or high-current arc (several hundred A) or plasma arc torch, in which the gas temperature inside the arc torch usually reaches over 10,000 K [34]. Compared to non-thermal plasma (i.e., with gas temperature close to the room temperature, such as corona discharge, glow discharge, and DBD), the average electron temperature is lower, but the electron density is much higher [35], important for efficient activation of chemical reactions.

* Corresponding author at: University of Science and Technology (UST), Republic of Korea.
** Corresponding author.
E-mail addresses: dhlee@kimm.re.kr (D.H. Lee), annemie.bogaerts@uantwerpen.be (A. Bogaerts).
[1] Co-first authors.

https://doi.org/10.1016/j.jcou.2020.101352
Received 25 July 2020; Received in revised form 25 September 2020; Accepted 18 October 2020
Available online 4 November 2020
2212-9820/© 2020 The Author(s). Published by Elsevier Ltd. This is an open access article under the CC BY-NC-ND license (http://creativecommons.org/licenses/by-nc-nd/4.0/).

Non-thermal arc plasmas can exist as (i) a two-dimensional (2D) gliding arc [7,9,36–44] or (ii) a three-dimensional (3D) arc plasma [9,21,25,31,45]. In a 2D gliding arc reactor, the arc is developed in a two-dimensional plane (i.e. between two blade-shaped electrodes). The arc column ignites at the shortest interelectrode position, and elongates as it moves towards larger interelectrode distances due to the gas flow, in which it cools down rapidly, until it extinguishes and a new arc is ignited at the shortest interelectrode distance. In this configuration, the reactant gas can however pass through the reactor without making contact with the arcs, hence limiting the gas fraction to be processed. To increase the contact probability between incoming gas and arcs, a 3D rotating arc reactor was introduced, in which the arcs move in three dimensions. The 3D arc technology has been more widely used for industrial applications than other arc configurations [32,46–48]. The notion of 3D bears the meaning that the arc is stabilized or suspended in three degrees of freedom, meaning a more complex, 3D shape of the reactor (i.e. tubular instead of planar shape), with specialized inlets and outlets for the gas flow.

Rotating arc plasma reactors have been widely employed for chemical activation of various gases [9,22,25,49–56]. In their basic configuration, they are constructed of a high-voltage electrode (or anode) enveloped by a grounded cathode. Besides a conventional rotating arc reactor with straight cylindrical grounded tube [49,51,54], a nozzle-type rotating arc reactor with a nozzle as grounded electrode has been developed as well [22,25,50,52,57]. In addition, there exist other types of 3D arc reactors, e.g., referred to as vortex stabilized gliding arc discharge or gliding arc plasmatron [21,27–29,31,33,58–61]. In all of these 3D arc reactors, the arcs rotate in 3D space by a swirling flow inlet or by a magnetic field [54,62]. Experiments revealed that the energy efficiency of gas activation in a nozzle-type rotating arc reactor or vortex stabilized gliding arc plasmatron is higher than in a conventional rotating arc reactor [21,22,56,57]. Thus, the arc plasma reactor geometry can have a significant effect on the efficiency of chemical reactions.

In this work, we compare in detail two types of rotating arc reactors: a conventional rotating arc and a nozzle-type rotating arc. We investigate the effect of the reactor geometry on the chemical reaction performance for DRM. To explain the difference in performance, we study the electrical and thermal characteristics. Besides experiments, we also apply several modelling approaches, to evaluate the gas flow dynamics, heat transfer and plasma characteristics of both types of rotating arc reactors. We selected both a non-reacting flow condition (i.e., an argon/nitrogen mixture, at 8 standard litre per minute (SLPM) of argon and 8 SLPM of nitrogen) and a reacting flow condition (DRM). The non-reacting flow condition was used to investigate the effect of the reactor geometry on the thermal balance, while the reacting flow condition was used as a model reaction for studying the fuel conversion efficiency in both reactors.

2. Experiments

2.1. Reactor geometries

The conventional rotating arc reactor was constructed with a conical high-voltage electrode (15 mm in diameter at its full width) made of copper, enveloped by a cylindrical grounded electrode (17 mm inner diameter) made of stainless steel. Hence, the narrowest gap between the electrodes, where the arc was ignited, was approximately 1 mm. At stable conditions and high electrical power, the arc is anchored between the high-voltage electrode tip and the ground, as shown in Fig. 1a. Because the arc is focused at the high-voltage electrode tip, this can cause a hot spot development. For this reason, a water-cooled anode was used. The water cooling was not applied to the grounded electrode because of the moving arc spot at the grounded electrode. A thermocouple (TC) was located downstream the reactor, 100 mm from the high-voltage electrode bottom, to measure the downstream gas temperature, as shown in Fig. 1a.

The nozzle-type rotating arc reactor was created by modifying the geometry of the conventional reactor by adding a narrowing nozzle with a diameter of 8 mm, while the other geometrical parameters remained unchanged (Fig. 1b). The distance between the high-voltage electrode tip and nozzle was designed to be approximately 15 mm. The ignition procedure was similar in both reactors: the arc discharge was ignited at the smallest gap between the electrodes (1 mm gap). The main difference was the arc dynamics at the stable condition (after ignition), discussed in the following sections. Even though the downstream temperature measured by the TC does not reflect the actual gas temperature in the reaction volume, it provides some insight and a relative comparison of the gas temperatures inside the reaction volume of both plasma reactors.

2.2. Experimental setup and methodology

An AC plasma power supply that can support an operating arc voltage of several kV with a frequency of 20 kHz was adopted to generate the rotating arcs. The AC power supply provides high voltage transformation driven by sinusoidal wave input and includes the function of the ballast resistor. We used a Tektronix P6015A high voltage probe (1000:1) and Tektronix TCP303 current probe to measure the waveforms of voltage and current, using an oscilloscope (Tektronix TDS5054B). The plasma power was calculated by direct integration of the product of voltage and current, as expressed in Eqn. (1). The sampling rate of the voltage and current was 2 MHz, which is sufficient to perform a direct integration considering the AC frequency of 20 kHz.

$$Power = \frac{1}{T}\int V \cdot I \, dt \ (\mathrm{W}) \tag{1}$$

Here, V and I denote the voltage (V) and current (A), respectively.

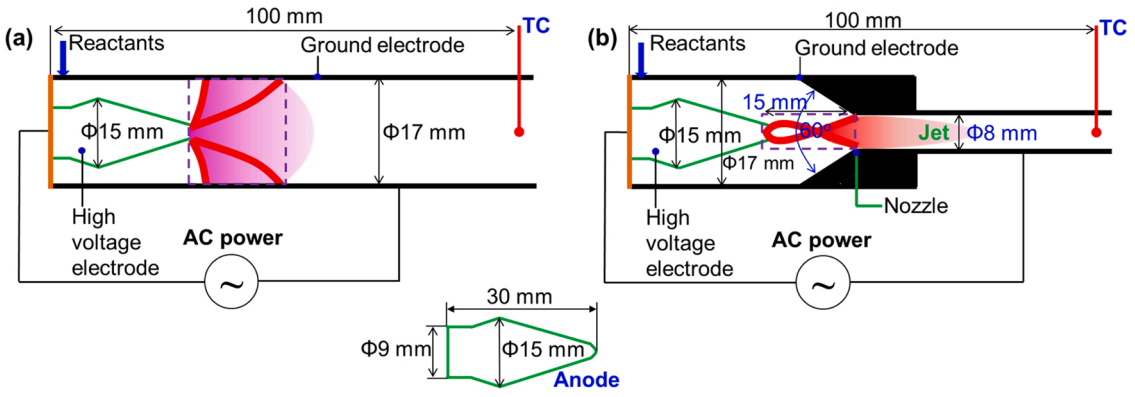

Fig. 1. (a) Conventional rotating arc reactor, (b) Nozzle-type rotating arc reactor.

For the reacting flow condition, we selected a mixture of $CH_4/CO_2/N_2$ (i.e. $CH_4 = 2$ SLPM, $CO_2 = 6$ SLPM, and $N_2 = 8$ SLPM) to create an arc discharge in the reactors. The presence of N_2 in the reactant mixture was required to obtain a stable arc discharge in the conventional rotating arc reactor. The main outlet gases included CH_4, CO_2, CO, H_2, N_2, H_2O, and other hydrocarbons (mainly. C_2H_6, C_2H_4, and C_2H_2). After H_2O was removed by a cold trap, the product was analysed by a micro gas chromatograph (490 Micro GC) that can measure H_2, O_2, N_2, CH_4, CO, CO_2, and hydrocarbon species up to carbon number of 4.

The conversions of CH_4 and CO_2 were calculated by Eqs. (2) and (3).

$$X_{CH_4} = \left(\frac{[C_{CH_4}]_{in} - \alpha[C_{CH_4}]_{out}}{[C_{CH_4}]_{in}}\right) \cdot 100\ (\%) \tag{2}$$

$$X_{CO_2} = \left(\frac{[C_{CO_2}]_{in} - \alpha[C_{CO_2}]_{out}}{[C_{CO_2}]_{in}}\right) \cdot 100\ (\%) \tag{3}$$

Here, α is the correction factor to account for gas expansion, calculated by Eq. (4):

$$\alpha = \frac{[C_{N_2}]_{in}}{[C_{N_2}]_{out}} \tag{4}$$

where $[C_{CH_4}]_{in}$, $[C_{CO_2}]_{in}$, and $[C_{N_2}]_{in}$ are the concentrations (in%) of CH_4, CO_2, and N_2, respectively, measured after passing through the reactor without plasma; $[C_{CH_4}]_{out}$, $[C_{CO_2}]_{out}$, and $[C_{N_2}]_{out}$ represent the concentrations of CH_4, CO_2, and N_2, respectively, in the effluent gas with plasma.

The selectivity of H_2, CO, and C_2 hydrocarbons (C_2H_y) was defined as follows:

$$S_{H_2} = \left(\frac{\alpha[C_{H_2}]_{out}}{2 \cdot [C_{CH_4}]_{in} \cdot \frac{X_{CH_4}}{100}}\right) \cdot 100\ (\%) \tag{5}$$

$$S_{CO} = \left(\frac{\alpha[C_{CO}]_{out}}{[C_{CH_4}]_{in} \cdot \frac{X_{CH_4}}{100} + [C_{CO_2}]_{in} \cdot \frac{X_{CO_2}}{100}}\right) \cdot 100\ (\%) \tag{6}$$

$$S_{C_2H_y} = \left(\frac{\alpha\left(2 \cdot [C_{C_2H_y}]_{out}\right)}{[C_{CH_4}]_{in} \cdot \frac{X_{CH_4}}{100} + [C_{CO_2}]_{in} \cdot \frac{X_{CO_2}}{100}}\right) \cdot 100\ (\%) \tag{7}$$

here $[C_{H_2}]_{out}$, $[C_{CO}]_{out}$, and $[C_{C_2H_y}]_{out}$ denote the concentrations of H_2, CO, and hydrocarbons (C_2H_y), respectively, in the effluent gas with plasma; y denotes the number of H atoms in the hydrocarbons ($y = 2$, 4, or 6).

The energy efficiency (in%) was calculated by Eq. (8), which was adopted from previous studies [22,30,52,56,63–68].

$$\eta = \frac{\alpha\left(\frac{[C_{CO}]_{out}}{100} \cdot LHV_{CO} + \frac{[C_{H_2}]_{out}}{100} \cdot LHV_{H_2}\right)}{\frac{[C_{CH_4}]_{in}}{100} \cdot \frac{X_{CH_4}}{100} \cdot LHV_{CH4} + SEI} \cdot 100(\%) \tag{8}$$

where LHV (kJ/L) is the lower heating value [69] and SEI (kJ/L) *is* the specific energy input, defined in Eqn. (9):

$$SEI = \frac{\frac{P_{in} \cdot 60}{1000}}{F^{in}_{CH_4} + F^{in}_{CO_2} + F^{in}_{N_2}}\ (kJ \Big/ L) \tag{9}$$

where P_{in} is the discharge power (in W); and $F^{in}_{CH_4}$, $F^{in}_{CO_2}$, and $F^{in}_{N_2}$ are the flow rates of the CH_4, CO_2, and N_2 inlets (SLPM), respectively. In this power supply, we can control the value of supplied power (or set power); an increase in the supplied power mainly results in an increase of current with an insignificant change in voltage, therefore the plasma power (measured by the oscilloscope) is increased.

Each experiment was carried out three times, and a propagation of uncertainty was implemented to the experimental results to calculate the error bars.

3. Results and discussion

3.1. Performance of both reactors for dry reforming of methane (DRM)

We studied the performance of both reactors for DRM in a wide range of SEI values, to evaluate the effect of the difference in reactor geometry. Fig. 2 shows that the conversions in the nozzle-type rotating arc reactor were much higher than in the conventional reactor. For example, at an SEI of 5 kJ/L, the CH_4 and CO_2 conversions in the nozzle-type reactor were 74% and 49%, respectively, while they were only 40% and 28%, respectively, in the conventional reactor. This difference can be explained by the thermal analysis of both reactors, i.e., less thermal losses to the walls and thus more energy available for the chemical reactions in the nozzle-type reactor, which will be elucidated in the following sections. The conversion rises upon higher electrical power due to the higher gas temperature and electron density, which is consistent with calculation results from thermodynamic equilibrium [22,70]. Furthermore, the power density in the contraction area of the nozzle-type reactor is higher, which can lead to higher electron density (leading to more electron impact-associated conversion), and overall, to a higher thermal conversion.

In addition, the energy efficiency calculated by Eq. (8) (see Fig. 3) is higher in the nozzle-type reactor, i.e., around 53% versus 36–44% (in the SEI range of 2.8–5.1 kJ/L) for the conventional reactor. The difference is slight higher at higher SEI values.

The values achieved in the nozzle-type rotating arc reactor, i.e., energy efficiency of around 53% at maximum conversions of CH_4 and CO_2 of 74% and 49%, are comparable or higher than the reported results in most gliding arc plasmas (typically around 28% energy efficiency at CH_4 and CO_2 conversion of 40% and 31%) [38,71]. The energy efficiency reported in this study is somewhat lower than in a gliding arc plasmatron (66%) [21], but the conversions in the latter were much lower (i.e., ca. 45% for CH_4 and slightly above 20% for CO_2). Also when comparing to the literature-wide overview presented by Snoeckx and Bogaerts [4], the nozzle-type rotating arc plasma is clearly among the most promising types of plasma for dry reforming of methane.

Analysis of the product selectivity indicates that there was roughly no difference in the reaction pathways in both reactors. The main products, i.e., hydrogen and carbon monoxide, showed virtually no difference in both reactors, but the hydrocarbons, especially C_2H_2, exhibited a difference of 0.2–1.6% (i.e., the same difference as in the CO selectivity), see Fig. 4. We attribute this small difference to the somewhat different residence time, i.e., the time for the reactants to pass through the arc volume. Indeed, the arcs cover a larger volume in the conventional reactor than in the nozzle-type reactor, as becomes clear from Fig. 5 below. The difference almost disappears upon increasing SEI value, where thermal processes compensate for the effect of the shorter residence time. The carbon balance is as high as 98 —99.6%, depending on the experimental conditions.

3.2. Arc dynamics and current–voltage characteristics

To understand the reason for the different performance of both reactors, we investigated the behaviour of the arcs inside the reactor. The development of the arc length inside a closed 3D geometry reactor is more difficult to observe than in a 2D gliding arc reactor. However, the change of the arc length can be partially determined based on the current-voltage characteristics: an increase in arc length leads to a higher voltage [41,51,52].

In both reactors, the arc discharge was ignited at the smallest gap between the electrodes (1 mm gap) to elongate to the high voltage

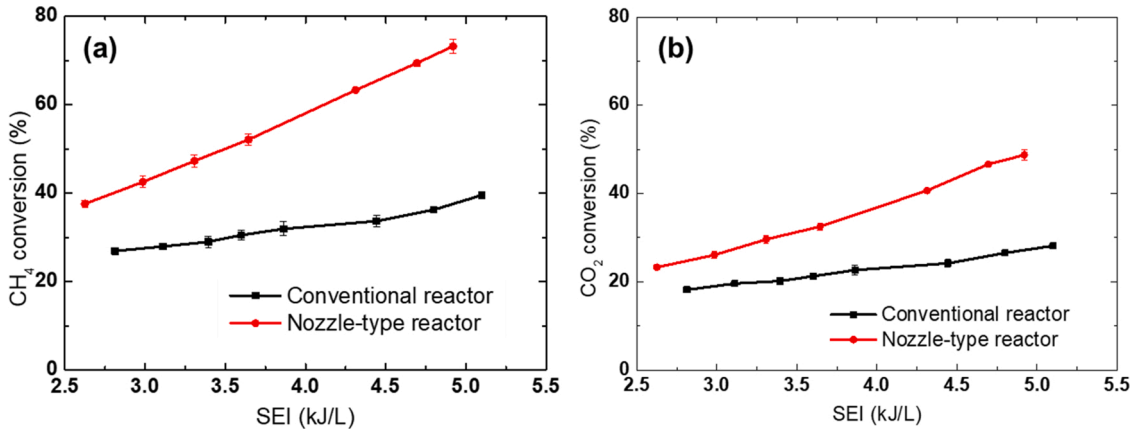

Fig. 2. Conversions in both reactors: (a) CH_4 conversion and (b) CO_2 conversion, as a function of SEI, for a $CO_2/CH_4/N_2$ mixture, with $CH_4 = 2$ SLPM, $CO_2 = 6$ SLPM, $N_2 = 8$ SLPM, and varying power between 750 W and 1360 W. The error bars (based on three independent experiments) are sometimes too small to be visible.

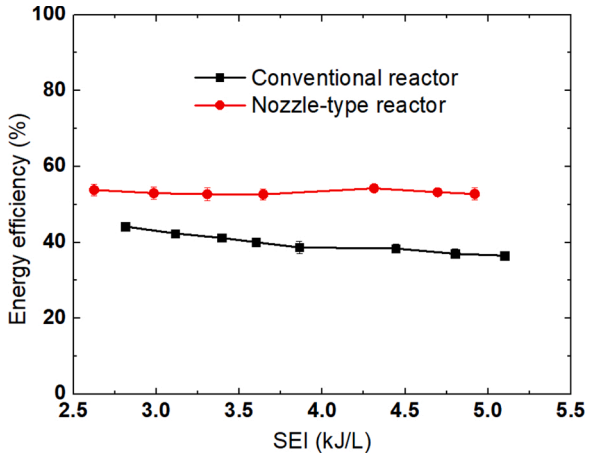

Fig. 3. Energy efficiency in both reactors, as a function of SEI, for the same conditions as in Fig. 2. The error bars (based on three independent experiments) are sometimes too small to be visible.

electrode tip. However, there is a significant difference in the arc behaviour in both reactors after ignition, which is partly indicated by the oscillograms of current and voltage, presented in Fig. 5. In the conventional rotating arc reactor, the arc length changes periodically, revealed by a periodic change of current and voltage (about a frequency of about 100 Hz); see Fig. 5a. This frequency does not depend on the SEI condition (ranged from 2.6 —5.0 kJ/L in this study), however, it strongly depends on the total flowrate. For example, when the total flowrate increased from 16 SLPM ($CH_4 = 2$ SLPM, $CO_2 = 6$ SLPM, and $N_2 = 8$ SLPM) to 32 SLPM ($CH_4 = 4$ SLPM, $CO_2 = 12$ SLPM, and $N_2 = 16$ SLPM), this frequency increased from approximately 100 Hz to about 200 Hz.

In the nozzle-type rotating arc reactor, the arcs are stably anchored between the high voltage electrode tip and the nozzle. Therefore, the arc length mostly remains unchanged, as evidenced by a more stable oscillogram of the current and voltage; see Fig. 5b. Note that the glitches observed in the nozzle-type reactor indicate that the foot of the arc column on the ground is still moving, but the moving distance is small. In the conventional rotating arc reactor, the end-point of the arc column on the grounded electrode moves in a large area, resulting in significant changes in the arc length and dispersion of the arcs in a large area, while the arc is clearly more focused in a smaller volume in the nozzle-type rotating arc reactor. This has important consequences for efficient energy use and reduced heat losses, as will be discussed in section 4 below, which can explain the better performance of the nozzle-type rotating arc reactor, as shown in previous section. Note that selecting a suitable distance from the high voltage electrode tip to the nozzle (i.e., 15 mm indicated in Fig. 1b) is also important to have stably anchoring arcs. If this distance is beyond the limit (i.e., longer than 25 mm), arcs cannot be stably anchored between the high voltage tip and the nozzle because a limitation of arc length that can be supported by the potential provided by the power supply (high voltage transformer).

The current and voltage were directly measured by an oscilloscope;

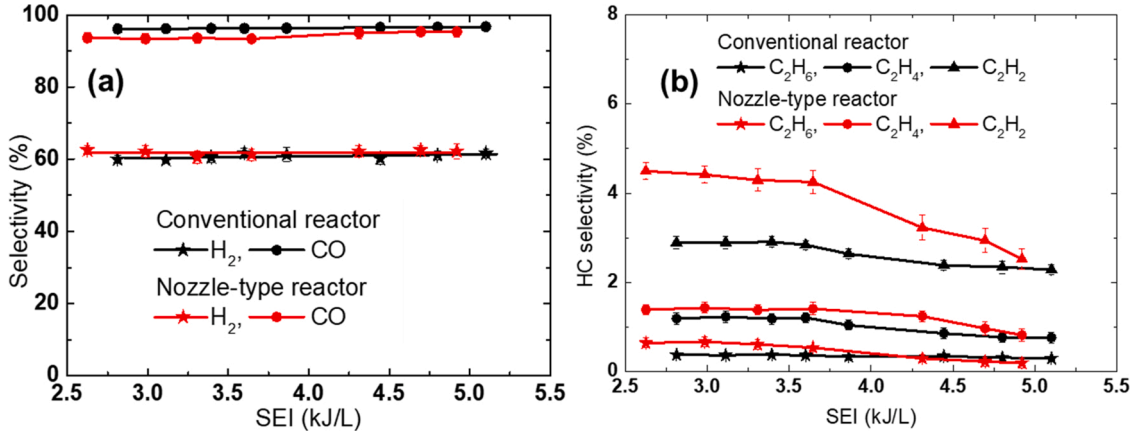

Fig. 4. Selectivity of (a) the synthesis gas components (CO and H_2) and (b) the main hydrocarbons, in both reactors, as a function of SEI, for the same conditions as in Fig. 2. The error bars (based on three independent experiments) are sometimes too small to be visible.

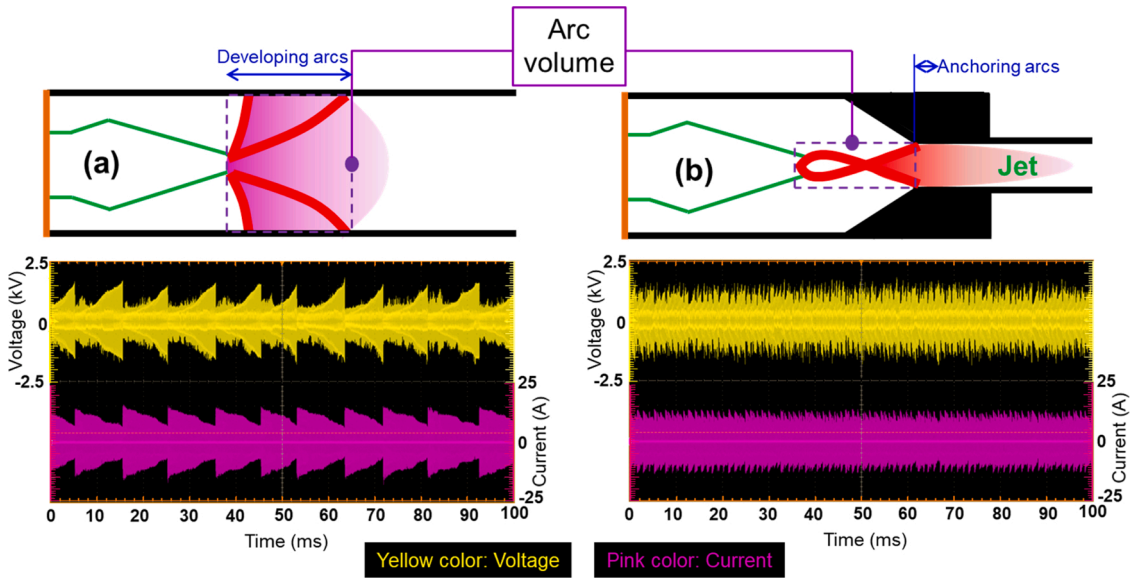

Fig. 5. Schematic pictures and oscillograms of the voltage (yellow color) and current (pink color) in the conventional (a) and nozzle-type (b) rotating arc reactor, for the same gas mixture as in Fig. 2, an electrical power of 1000 W, and overall time span of 100 milliseconds. The volume occupied by the arcs is schematically indicated in both reactors by the purple dashed lines.

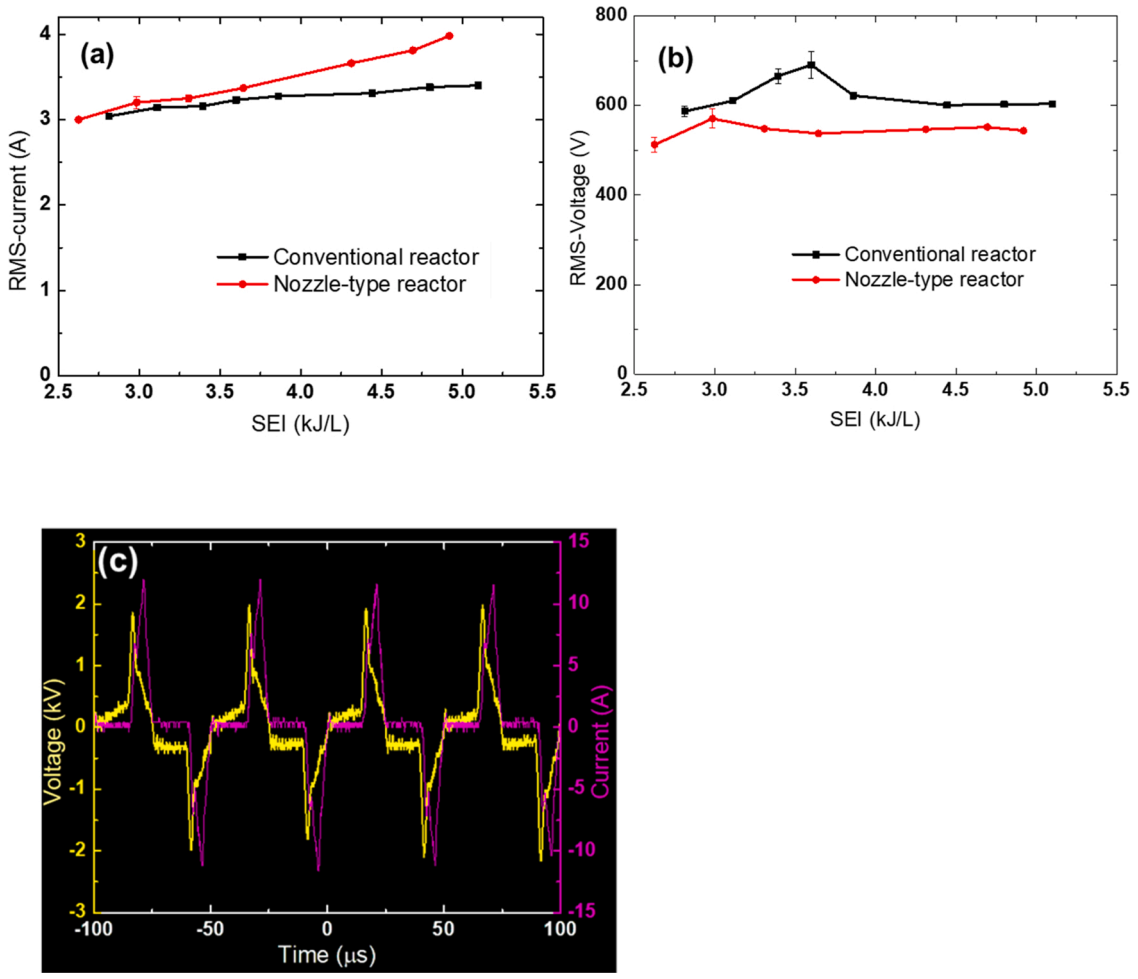

Fig. 6. RMS current (a) and voltage (b) as a function of SEI, in both reactors, for the same conditions as in Fig. 2. The error bars (based on three independent experiments) are sometimes too small to be visible, (c) current and voltage characteristics of several arc events in the nozzle-type rotating arc reactor, showing the slight phase difference between voltage and current.

the RMS-current and RMS-voltage are correlated to the average diameter and average length of the arc column, respectively. Although we cannot quantify the arc length and diameter from the current and voltage data, we can deduce the different arc shape from the current-voltage characteristics of both reactor geometries. The nozzle structure prevents further elongation of the arcs beyond the nozzle inlet, resulting in slightly shorter and thicker arc columns, as indicated by a slightly higher RMS-current and lower RMS-voltage in the nozzle-type reactor, see Fig. 6, because an increase in arc length leads to a higher voltage [40,41,52]. Fig. 6c showed the voltage rise and current decay in the arc discharge process. Because arc length (in the conventional reactor) is significantly and periodically changed, several arc events cannot exactly reflect the overall oscillograms of voltage and current. Therefore, several arc events in the nozzle-type rotating arc reactor were selected to describe the voltage increase and current decay.

3.3. Gas flow pattern inside the reactors

Fig. 7 shows the gas velocity streamlines in the 3D geometry for both reactors, calculated by solving the Navier–Stokes equations for a Newtonian fluid, i.e., the mass continuity equation (Eqn. (10)) and momentum continuity equation (Eqn. (11)). A turbulent RANS model (k-epsilon) was used. This means that the Navier-Stokes equations were coupled with two more transport equations, describing the turbulent kinetic energy (k_{Tu}) and the turbulent dissipation rate (ε), as described in more detail by Trenchev et al. [33].

$$\nabla \cdot \left(\rho \vec{u_g}\right) = 0 \tag{10}$$

$$\rho\left(\vec{u_g} \cdot \nabla\right)\vec{u_g} = \nabla \cdot \left[-p\vec{I} + (\mu + \mu_{Tu})\left(\nabla \vec{u_g} + \nabla\left(\vec{u_g}\right)^T\right) - \frac{2}{3}(\mu + \mu_{Tu})\left(\nabla \vec{u_g}\right)\vec{I} - \frac{2}{3}\rho k_{Tu}\vec{I}\right] + \vec{F} \tag{11}$$

Here, ρ is the gas density; $\vec{u_g}$ is the gas flow velocity vector; p is the gas pressure; μ is the dynamic viscosity of the fluid; μ_{Tu} is the turbulent viscosity of the fluid; k_{Tu} is the turbulent kinetic energy; I is the unity tensor; F is the body force vector, and superscript T stands for transposition.

The boundary conditions include four gas inlet flows defined as the gas flow normal velocity boundaries. The outlet is defined as a zero-gradient outflow boundary with no flux at the reactor wall and a no-slip condition. The RANS *k*-epsilon model is used for computing a variety of flow problems, and is considered to be accurate for most engineering applications [72].

16 SLPM of pure nitrogen was used for these calculations. The gas inlet was tangentially inserted into the reactor through four small holes 1 mm in diameter with a velocity greater than 100 m/s. The tangential inlet-flows form a high-velocity peripheral stream along the walls. Therefore, the tangential gas velocity near the wall is higher than at the reactor centre. There is no significant difference in the gas velocity streamlines in both reactors, so the gas flow profile cannot explain the different performance of both reactors.

3.4. Thermal distribution characteristics

The reason for the different performance of both reactors, as already mentioned above, can be found in the thermal characteristics. An arc plasma provides highly reactive species for activating chemical reactions and a high gas temperature for thermal activation. Because of the minor difference in current and voltage characteristics, as shown in Fig. 6, we expect the plasma chemistry arising from the electrical energy to be similar in both reactors. However, a modification of the reactor geometry may affect the thermal behaviour. We can write the energy balance by Eq. (12).

$$P_{in} = \omega P_{in} + (1 - \omega)P_{in} \tag{12}$$

Here ωP_{in} denotes the portion of electrical energy converted to thermal energy or heat and $(1 - \omega)P_{in}$ indicates the energy use other than the generation of heat. Therefore, ω is the thermal conversion coefficient that indicates how much electrical energy is transferred to thermal energy. This coefficient is assumed to be independent of the modification in reactor geometry, because of the small differences in current-voltage characteristics.

The thermal energy from the arc is converted into heat loss to the reactor body and kinetic energy of the gas species, see Eqn. (13),

$$Q = \omega P_{in} = Q_{loss} + Q_{gas} \tag{13}$$

where Q is the amount of thermal energy from the arc; Q_{loss} and Q_{gas} are the heat loss and kinetic energy of the gas species, respectively.

Because we expect the change in plasma chemistry induced by attachment of the nozzle downstream the reactor to be negligible, as revealed by the electrical characteristics, the effect of the nozzle should be mostly reflected in the thermal energy inside of the reactor. Indeed, the modification of the reactor geometry can lead to a significant change in heat losses to the reactor body. To investigate this in more detail, we developed a model for gas heating with an artificial heat source, mimicking the plasma arc.

The gas heating equation can be expressed as Eq. (14).

$$\rho C_p \frac{\partial T_g}{\partial t} + \rho C_p \vec{u_g} \cdot \nabla T_g - \nabla \cdot \left(k_{eff} \nabla T_g\right) = Q \tag{14}$$

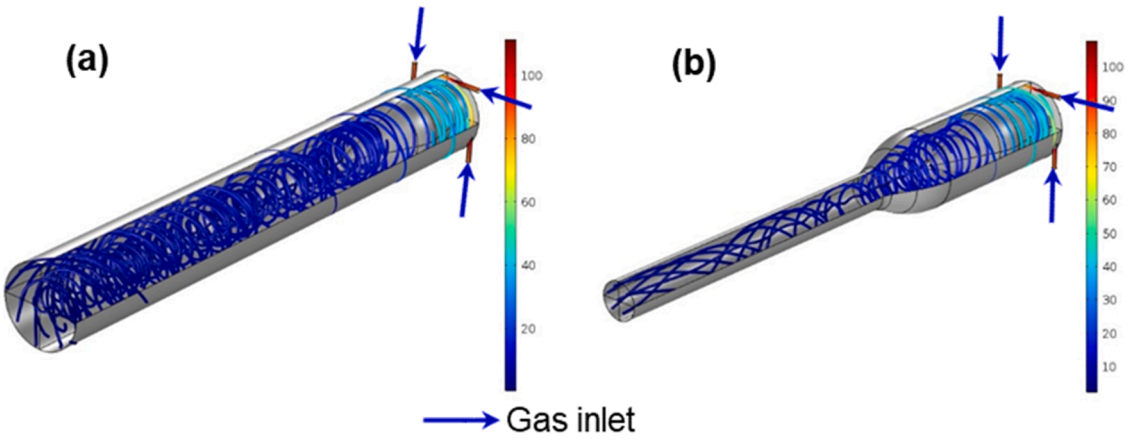

Fig. 7. Calculated streamlines of the gas velocity (in m/s) inside the conventional (a) and nozzle-type (b) rotating arc reactors, for an inlet gas flow rate of 16 SLPM. The blue arrows indicate the gas inlet positions. Note that the setup is turned around with respect to Fig. 1.

Here, ρ is the gas density; C_p is the heat capacity of the gas; k_{eff} is the effective temperature-dependent gas thermal conductivity (based on a material look-up table and turbulent enhancement) [60]; T_g is the gas temperature, and Q accounts for the gas heating owing to elastic and inelastic collisions between electrons and heavy particles in the plasma, or thermal energy converted from the arc to the reactant gas during the plasma process.

In our work, Q was replaced by an artificial heat source of 800 W, placed at the high-voltage electrode tip to study heat transfer. The circular artificial heat source has a Gaussian distribution gradient, as shown in Fig. 8.

Fig. 9a clearly demonstrates that the nozzle-type geometry exhibits a shield layer by the converging flow pattern for the high-temperature region, resulting in a larger volume with high temperature close to the high-voltage electrode tip. Therefore, the heat loss in this region in the nozzle-type reactor can be effectively reduced. In our calculation, heat losses at the walls are not accounted for; the walls are adiabatic. An exact count of heat loss is challenging, therefore we provided a relative comparison of the heat loss in the two reactors based on the wall temperature (inside wall temperature) by using Eq. (15); a higher wall temperature should result in a higher heat loss through the reactor wall.

$$q_{loss} = \int_A A_i \frac{T_{wall_i} - T_{room}}{\frac{L}{k} + \frac{1}{h}} \approx \int_A hA_i (T_{wall_i} - T_{room}) \quad (15)$$

Because of k>>h (k is the thermal conductivity of reactor wall materials, h is the convective heat transfer coefficient of the surrounding environment, L is the thickness of the reactor wall, A denotes the studied area).

The calculated temperature profiles in a cross section of both reactors are illustrated in Fig. 9b. The wall temperature of the conventional reactor is approximately 1650 K, which is much higher than in the nozzle-type reactor (700 K), while the temperature in the center is calculated to be much higher in the nozzle-type reactor (above 4900 K vs about 3330 K for the conventional reactor). Hence, the nozzle-type reactor keeps its plasma energy in a confined volume at higher temperature, which is beneficial for gas activation, and reduces the heat losses to the walls, as discussed below in more detail.

We tried to validate our calculated gas temperature profiles of Fig. 9 by measuring the temperatures at various locations (see TC1—TC7 in Fig. 10) at the reactor surface, as well as the gas downstream temperature (TC). A static flow condition of non-reacting flow of argon and nitrogen was used for this investigation.

Fig. 10 shows that the gas temperature measured by the TC downstream the nozzle-type reactor was much higher than downstream the conventional rotating arc reactor (i.e. 965 °C compared to 380 °C), which points out that the energy was more efficiently used for heating the gas. Although the downstream gas temperatures were measured at similar distances from the high-voltage electrode, the gas residence time, i.e., the time the gas needs in order to pass from the inlet position to the position of the TC, is different in both reactors. The gas residence time in the nozzle-type reactor is shorter than in the conventional reactor (i.e., approximately 45 milliseconds in the nozzle-type reactor compared to 85 milliseconds in the conventional reactor) due to the difference in reactor geometry. Nevertheless, the difference in downstream gas temperatures is sufficiently high to conclude that the energy is more efficiently used for heating the gas in the nozzle-type reactor than in the conventional reactor.

The thermal loss to the reactor body can be deduced from the reactor surface temperatures. Fig. 10 shows that the surface temperatures in the region covered by the arcs (i.e. measured by TC1–TC4) in the nozzle-type reactor were lower than in the conventional reactor, which points towards lower heat losses. These surface temperatures, measured by TC1–TC4, were located at positions with similar outer diameters in both reactors. The measured reactor surface temperatures and downstream gas temperatures provide solid evidence that the reactor geometry modification (i.e., nozzle-type) enhances the kinetic energy of the gas (Q_{gas}) and reduces thermal losses (Q_{loss}).

Further analysis of the reactor surface temperatures reveals that in the conventional rotating arc reactor, the surface temperatures in the region covered by the arcs (i.e. from TC1 to TC4) were higher than in the downstream region of the arcs (i.e. from TC5 to TC7), which indicates that the gas temperature downstream was low. In comparison, the reactor surface temperature in the nozzle-type reactor reaches its maximum at the position of TC6, which shows that the region covered by the arcs and near the arcs was well insulated by a cold gas layer, resulting in reduced heat loss through the reactor walls. In addition, the gas temperature in the jet region (downstream the arcs) was much higher in the nozzle-type reactor, as evidenced by the higher temperatures of TC5–TC7 and the downstream gas.

3.5. Arc plasma characteristics

Finally, to obtain more insight in the plasma characteristics and arc behaviour, we show in Fig. 11 the calculated plasma (or electron)

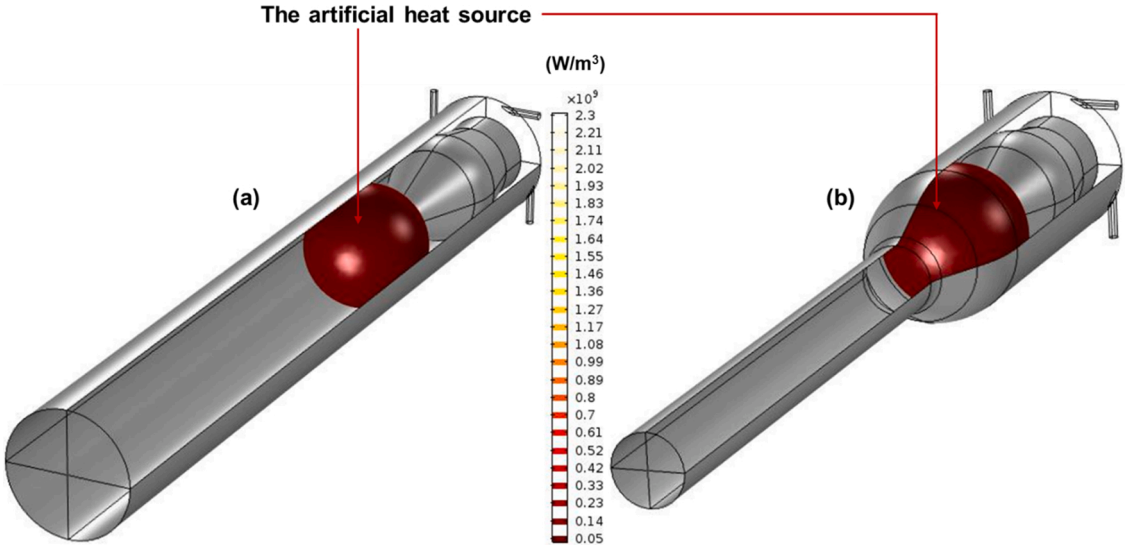

Fig. 8. Distribution of the circular artificial heat source of 800 W, with a Gaussian distribution gradient inside the reactors: conventional (a) and nozzle-type (b) rotating arc reactor.

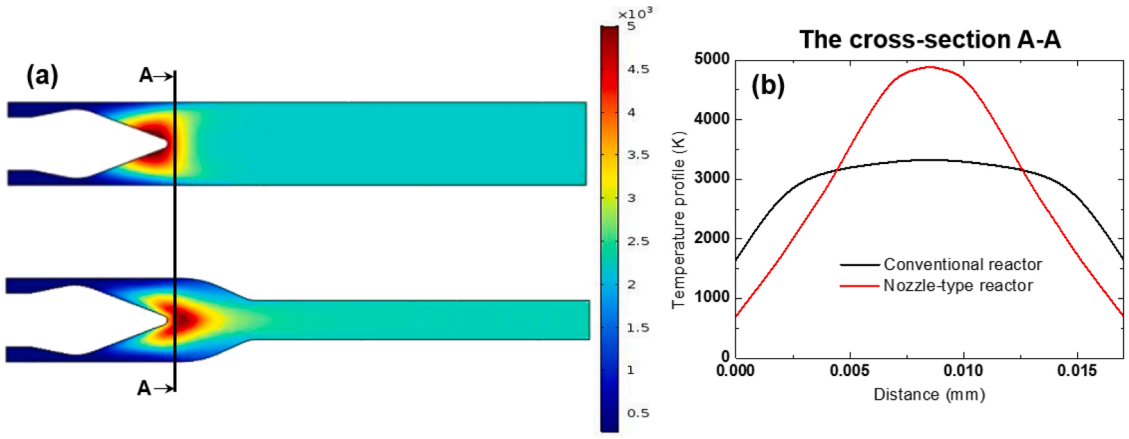

Fig. 9. (a) Calculated gas temperature distribution in the conventional and nozzle-type reactor (upper and lower panel) and (b) gas temperature profiles in a cross-section (A-A) in the arc region of both reactors.

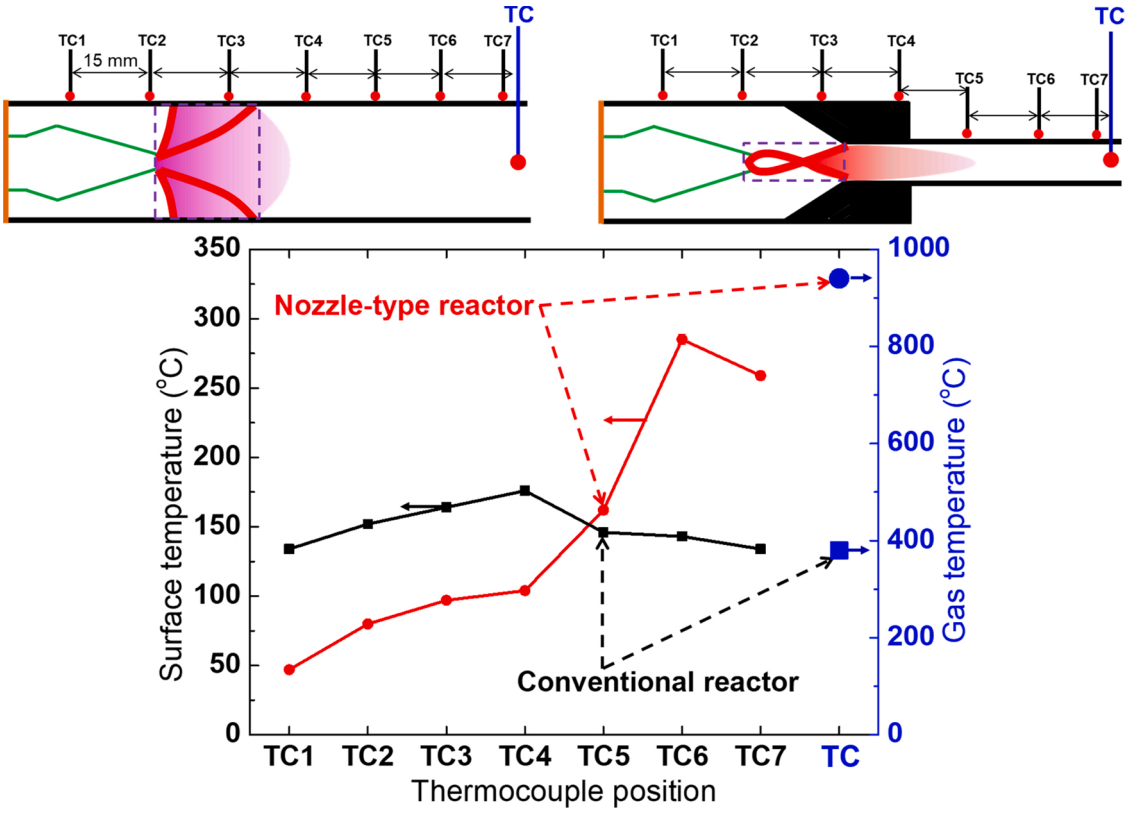

Fig. 10. Comparison of the reactor surface temperatures and downstream gas temperature in both reactors, for an argon/nitrogen mixture (8 SLPM of argon and 8 SLPM of nitrogen), and electrical power of 800 W. The distance between the surface thermocouples is 15 mm. The error bars (based on three independent experiments) were included in the graphs, but they were too small to be visible.

density, as obtained from the fluid plasma model. The results are shown for the conventional reactor, but they would be the same for the nozzle-type reactor, as they focus on the region around the high-voltage electrode, where the effect of the nozzle is not visible. Hence, the purpose of these calculations is not to explain the different performance of both reactors, which is presented in previous section, but rather to obtain additional insight in the general plasma characteristics. Due to computational limitations, the plasma chemistry in the model is limited to Ar gas, based on reference [33]. We realize that the model is for argon, so it might be different from the experiments, but developing this model in the CO_2/CH_4 mixture with all the chemistry would lead to unacceptable calculation times. Moreover, the arc behaviour can be very similar between different gases, as proven before [59] to be accurate enough for estimating the arc rotation. The calculated plasma density is around 10^{21} m^{-3}, which is typical for atmospheric pressure arc discharges [33, 60]. We observe a smooth rotation of the arc, driven by the convective flow. Note that the flow vector will drive a convective heat transport (see Fig. 7), forcing the heating processes in the area around the conical high-voltage electrode, as shown in Fig. 9. The electron temperature was calculated to be 2.5 eV. Note that we only present the electron density and electron temperature, as we use an argon-based fluid plasma model with a reduced chemistry set, including only one type of ions (Ar^+). The model is quasi-neutral, which means that the electron density matches the ion density. Therefore, the model only calculates the electron and

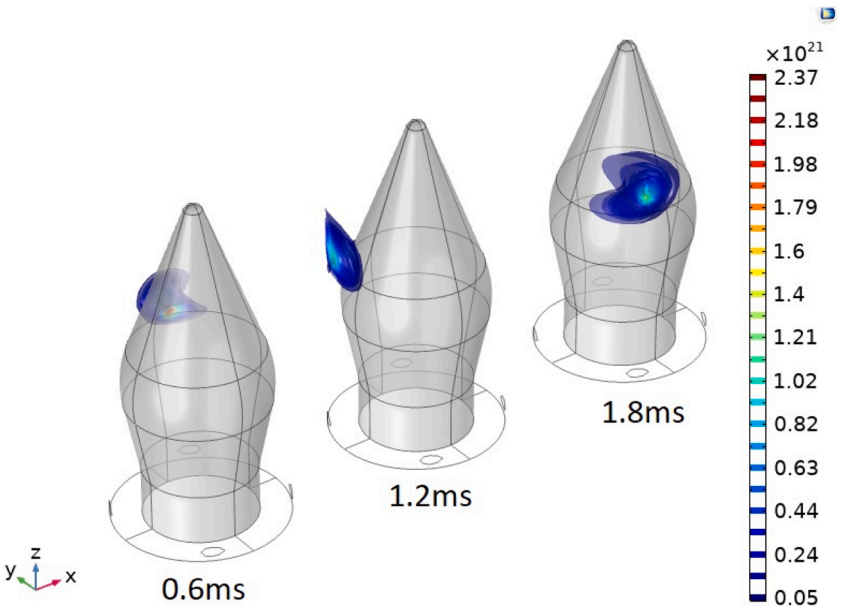

Fig. 11. Calculated plasma (or electron) density (in m^{-3}), by means of the plasma model, from the early stage (0.6 ms) to ½ revolution (1.8 ms), to visualize the arc rotation, for the conventional rotating arc reactor. The ground electrode is hidden in the figure, for better visibility.

Ar^+ ion density, electron temperature, and gas temperature. We refer to reference [33] for more information. The ground electrode is hidden in the figure, for better visibility.

Fig. 12 depicts the calculated gas temperature for the argon plasma model. Note that this is the peak (center) gas temperature. Values up to 3000 K and above are obtained, which are in the typical range of atmospheric arc discharges [33,60]. Note that the region of elevated gas temperature is somewhat wider than the strict plasma region as defined by the plasma density in Fig. 11 above, due to convective heat transfer from the hot plasma to its (direct) surroundings.

4. Conclusion

We studied a 3D rotating arc reactor in two different configurations, i.e., conventional and nozzle-type reactor, by means of experiments and modelling. The difference in reactor geometry affects the thermal balance, i.e., gas kinetic energy against heat loss to the walls. The nozzle-type reactor significantly reduces the convective heat transfer through the reactor walls by flow-induced thermal insulation, thus enhancing the efficiency of using the applied plasma power for the gas conversion, explaining the higher CO_2 and CH_4 conversions and energy efficiency for DRM.

The significant enhancement of the conversions and energy efficiency by reducing thermal losses to the reactor walls indicates the importance of thermal activation of the gases in DRM in the arc plasma. Reactor design optimization can be used to control the energy use and limit the energy losses in arc plasma technology. This study provides important insights for optimizing arc plasma reactors for other chemical reactions as well.

Using a combination of different modelling approaches gives us a

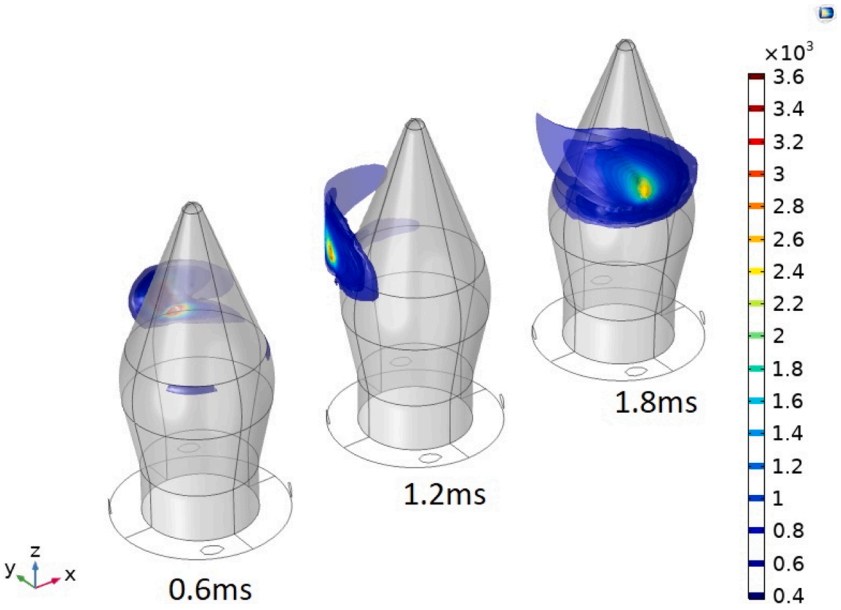

Fig. 12. Calculated gas temperature (in K) by means of the plasma model, from the early stage (0.6 ms) to ½ revolution (1.8 ms) for the conventional rotating arc reactor. The ground electrode is hidden in the figure, for better visibility.

deeper insight in the plasma behaviour. The fluid dynamics model accurately describes the gas flow behaviour in both reactors, while the heat transfer model can clearly explain why the nozzle-type reactor performs much better. Finally, the fluid plasma model provides more insight in the plasma parameters, such as electron density and temperature, and the arc motion.

Author statement

Duy Khoe Dinh and Dae Hoon Lee: Designing plasma reactors, selecting reaction conditions, performing experiments, analyzing the data, and writing portions of the manuscript. Georgi Trenchev: Modeling to give insights into plasma characteristics and writing portions of the manuscript. Annemie Bogaerts and Dae Hoon Lee: Writing, reviewing, and revising.

Declaration of Competing Interest

The authors report no declarations of interest.

Acknowledgments

This work is supported by the Institutional research program (NK225F and NG0340) of the Korea Institute of Machinery and Materials.

References

[1] J. Reece, J Reece Roth, 1995. https://doi.org/10.1016/j.rser.2014.07.134.
[2] A. Fridman, Plasma Chem. Plasma Process. (2007).
[3] D.H. Lee, Y.-H. Song, K.-T. Kim, S. Jo, H. Kang, Current state and perspectives of plasma applications for catalyst regeneration, Catal. Today 337 (2019) 15–27, https://doi.org/10.1016/j.cattod.2019.04.071.
[4] R. Snoeckx, A. Bogaerts, Plasma technology-a novel solution for CO2 conversion? Chem. Soc. Rev. 46 (2017) 5805–5863, https://doi.org/10.1039/c6cs00066e.
[5] H.H. Kim, Nonthermal plasma processing for air-pollution control: a historical review, current issues, and future prospects, Plasma Process. Polym. 1 (2004) 91–110, https://doi.org/10.1002/ppap.200400028.
[6] J.A. Andersen, J.M. Christensen, M. Østberg, A. Bogaerts, A.D. Jensen, Plasma-catalytic dry reforming of methane: screening of catalytic materials in a coaxial packed-bed DBD reactor, Chem. Eng. J. 397 (2020) 125519, https://doi.org/10.1016/j.cej.2020.125519.
[7] S. Liu, D. Mei, L. Wang, X. Tu, Steam reforming of toluene as biomass tar model compound in a gliding arc discharge reactor, Chem. Eng. J. 307 (2017) 793–802, https://doi.org/10.1016/j.cej.2016.08.005.
[8] W. Wang, D. Mei, X. Tu, A. Bogaerts, Gliding arc plasma for CO2 conversion: better insights by a combined experimental and modelling approach, Chem. Eng. J. 330 (2017) 11–25, https://doi.org/10.1016/j.cej.2017.07.133.
[9] H. Zhang, W. Wang, X. Li, L. Han, M. Yan, Y. Zhong, X. Tu, Plasma activation of methane for hydrogen production in a N 2 rotating gliding arc warm plasma: a chemical kinetics study, Chem. Eng. J. 345 (2018) 67–78, https://doi.org/10.1016/j.cej.2018.03.123.
[10] B. Eliasson, M. Hirth, U. Kogelschatz, Ozone synthesis from oxygen in dielectric barrier discharges, J. Phys. D Appl. Phys. 20 (1987) 1421–1437, https://doi.org/10.1088/0022-3727/20/11/010.
[11] A. Starikovskiy, N. Aleksandrov, Plasma-assisted ignition and combustion, Prog. Energy Combust. Sci. 39 (2013) 61–110, https://doi.org/10.1016/j.pecs.2012.05.003.
[12] D.H. Lee, K.T. Kim, H.S. Kang, Y.H. Song, J.E. Park, Plasma-assisted combustion technology for NOx reduction in industrial burners, Environ. Sci. Technol. 47 (2013) 10964–10970, https://doi.org/10.1021/es401513t.
[13] S.H. Pyun, D.H. Lee, K.T. Kim, Y.H. Song, Application of plasma fuel reformer to an on-board diesel burner, Plasma Chem. Plasma Process. 36 (2016) 329–340, https://doi.org/10.1007/s11090-015-9672-3.
[14] E. El Ahmar, C. Met, O. Aubry, A. Khacef, J.M. Cormier, Hydrogen enrichment of a methane-air mixture by atmospheric pressure plasma for vehicle applications, Chem. Eng. J. 116 (2006) 13–18, https://doi.org/10.1016/j.cej.2005.10.005.
[15] J.R. Fincke, R.P. Anderson, T. Hyde, R. Wright, R. Bewley, D.C. Haggard, W. D. Swank, Plasma thermal conversion of methane to acetylene final report, Plasma Chem. Plasma Process. 22 (2000) 105–136, https://doi.org/10.2172/774309.
[16] L. Tong, R.G. Reddy, Synthesis of titanium carbide nano-powders by thermal plasma, Scr. Mater. 52 (2005) 1253–1258, https://doi.org/10.1016/j.scriptamat.2005.02.033.
[17] L. Tong, R.G. Reddy, Thermal plasma synthesis of SiC nano-powders/nano-fibers, Mater. Res. Bull. 41 (2006) 2303–2310, https://doi.org/10.1016/j.materresbull.2006.04.021.
[18] M. Kim, Y.H. Lee, J.H. Oh, S.H. Hong, B. Il Min, T.H. Kim, S. Choi, Synthesis of boron nitride nanotubes using triple DC thermal plasma reactor with hydrogen injection, Chem. Eng. J. 395 (2020) 125148, https://doi.org/10.1016/j.cej.2020.125148.
[19] K. Shinoda, H. Murakami, Y. Sawabe, K. Saegusa, Ultrafast production of silicon via aluminothermic reduction of tetrachlorosilane in a thermal plasma jet, Chem. Eng. J. 198–199 (2012) 61–64, https://doi.org/10.1016/j.cej.2012.05.093.
[20] B. Yan, P. Xu, C.Y. Guo, Y. Jin, Y. Cheng, Experimental study on coal pyrolysis to acetylene in thermal plasma reactors, Chem. Eng. J. 207–208 (2012) 109–116, https://doi.org/10.1016/j.cej.2012.05.111.
[21] E. Cleiren, S. Heijkers, M. Ramakers, A. Bogaerts, Dry reforming of methane in a gliding arc plasmatron: towards a better understanding of the plasma chemistry, ChemSusChem. 10 (2017) 4025–4036, https://doi.org/10.1002/cssc.201701274.
[22] D.K. Dinh, S. Choi, D.H. Lee, S. Jo, K.T. Kim, Y.H. Song, Energy efficient dry reforming process using low temperature arcs, Plasma Process. Polym. 15 (2018) 1700203, https://doi.org/10.1002/ppap.201700203.
[23] X. Tao, M. Bai, Q. Wu, Z. Huang, Y. Yin, X. Dai, CO 2 reforming of CH 4 by binode thermal plasma, Int. J. Hydrogen Energy 34 (2009) 9373–9378, https://doi.org/10.1016/j.ijhydene.2009.09.048.
[24] L. Bromberg, D.R. Cohn, A. Rabinovich, C. O'Brien, S. Hochgreb, Plasma reforming of methane, Energy Fuels 12 (1998) 11–18, https://doi.org/10.1021/ef9701091.
[25] D.H. Lee, K.-T. Kim, H.S. Kang, S. Jo, Y.-H. Song, Optimization of NH3 decomposition by control of discharge mode in a rotating arc, Plasma Chem. Plasma Process. 34 (2014) 111–124, https://doi.org/10.1007/s11090-013-9495-z.
[26] W. Wang, B. Patil, S. Heijkers, V. Hessel, A. Bogaerts, Nitrogen fixation by gliding arc plasma: better insight by chemical kinetics modelling, ChemSusChem. 10 (2017) 2145–2157, https://doi.org/10.1002/cssc.201700611.
[27] M. Ramakers, S. Heijkers, T. Tytgat, S. Lenaerts, A. Bogaerts, Combining CO2 conversion and N2 fixation in a gliding arc plasmatron, J. CO2 Util. 33 (2019) 121–130, https://doi.org/10.1016/j.jcou.2019.05.015.
[28] J. Slaets, M. Aghaei, S. Ceulemans, S. Van Alphen, A. Bogaerts, CO2 and CH4 conversion in "real" gas mixtures in a gliding arc plasmatron: How do N2 and O2 affect the performance? Green Chem. 22 (2020) 1366–1377, https://doi.org/10.1039/c9gc03743h.
[29] M. Ramakers, G. Trenchev, S. Heijkers, W. Wang, A. Bogaerts, Gliding arc plasmatron: providing an alternative method for carbon dioxide conversion, ChemSusChem. 10 (2017) 2642–2652, https://doi.org/10.1002/cssc.201700589.
[30] T. Paulmier, L. Fulcheri, Use of non-thermal plasma for hydrocarbon reforming, Chem. Eng. J. 106 (2005) 59–71, https://doi.org/10.1016/j.cej.2004.09.005.
[31] C.S. Kalra, Y.I. Cho, A. Gutsol, A. Fridman, T.S. Rufael, Gliding arc in tornado using a reverse vortex flow, Rev. Sci. Instrum. 76 (2005) 025110, https://doi.org/10.1063/1.1854215.
[32] S.P. Gangoli, A.F. Gutsol, A.A. Fridman, A non-equilibrium plasma source: magnetically stabilized gliding arc discharge: I. Design and diagnostics, Plasma Sources Sci. Technol. 19 (2010) 065003, https://doi.org/10.1088/0963-0252/19/6/065003.
[33] G. Trenchev, S. Kolev, A. Bogaerts, A 3D model of a reverse vortex flow gliding arc reactor, Plasma Sources Sci. Technol. 25 (2016) 035014, https://doi.org/10.1088/0963-0252/25/3/035014.
[34] K. Bobzin, N. Bagcivan, L. Zhao, I. Petkovic, J. Schein, K. Hartz-Behrend, S. Kirner, J.L. Marqués, G. Forster, Modelling and diagnostics of multiple cathodes plasma torch system for plasma spraying, Front. Mech. Eng. China 6 (2011) 324–331, https://doi.org/10.1007/s11465-011-0125-2.
[35] Y. Ju, W. Sun, Plasma assisted combustion: dynamics and chemistry, Prog. Energy Combust. Sci. 48 (2015) 21–83, https://doi.org/10.1016/j.pecs.2014.12.002.
[36] L. Li, H. Zhang, X. Li, X. Kong, R. Xu, K. Tay, X. Tu, Plasma-assisted CO 2 conversion in a gliding arc discharge: improving performance by optimizing the reactor design, J. CO2 Util. 29 (2019) 296–303, https://doi.org/10.1016/j.jcou.2018.12.019.
[37] A. Fridman, S. Nester, L.A. Kennedy, A. Saveliev, O. Mutaf-Yardimci, Gliding arc gas discharge, Prog. Energy Combust. Sci. 25 (1999) 211–231, https://doi.org/10.1016/S0360-1285(98)00021-5.
[38] A. Indarto, J.-W. Choi, H. Lee, H.K. Song, Effect of additive gases on methane conversion using gliding arc discharge, Energy. 31 (2006) 2986–2995, https://doi.org/10.1016/j.energy.2005.10.034.
[39] W. Wang, A. Berthelot, S. Kolev, X. Tu, A. Bogaerts, CO2conversion in a gliding arc plasma: 1D cylindrical discharge model, Plasma Sources Sci. Technol. 25 (2016) 65012, https://doi.org/10.1088/0963-0252/25/6/065012.
[40] I.V. Kuznetsova, N.Y. Kalashnikov, A.F. Gutsol, A.A. Fridman, L.A. Kennedy, Effect of "overshooting" in the transitional regimes of the low-current gliding arc discharge, J. Appl. Phys. 92 (2002) 4231–4237, https://doi.org/10.1063/1.1505682.
[41] O. Mutaf-Yardimci, A.V. Saveliev, A.A. Fridman, L.A. Kennedy, Thermal and nonthermal regimes of gliding arc discharge in air flow, J. Appl. Phys. 87 (2000) 1632–1641, https://doi.org/10.1063/1.372071.
[42] F. Richard, J.M. Cormier, S. Pellerin, J. Chapelle, Physical study of a gliding arc discharge, J. Appl. Phys. 79 (1996) 2245–2250, https://doi.org/10.1063/1.361188.
[43] S. Kolev, A. Bogaerts, A 2D model for a gliding arc discharge, Plasma Sources Sci. Technol. 24 (2015) 15025, https://doi.org/10.1088/0963-0252/24/1/015025.
[44] Y. Xia, N. Lu, J. Li, N. Jiang, K. Shang, Y. Wu, Combined steam and CO2 reforming of CH4 for syngas production in a gliding arc discharge plasma, J. CO2 Util. 37 (2020) 248–259, https://doi.org/10.1016/j.jcou.2019.12.016.
[45] H. Zhang, X. Li, F. Zhu, K. Cen, C. Du, X. Tu, Plasma assisted dry reforming of methanol for clean syngas production and high-efficiency CO2 conversion, Chem. Eng. J. 310 (2017) 114–119, https://doi.org/10.1016/j.cej.2016.10.104.

[46] D.H. Lee, H. Kim, Y.H. Song, K.T. Kim, Plasma burner for active regeneration of diesel particulate filter, Plasma Chem, Plasma Process. 34 (2014) 159–173, https://doi.org/10.1007/s11090-013-9507-z.
[47] K. et Al., Plasma scrubber, US patent US8574504B2, 2013.
[48] S.H. Pyun, D.H. Lee, K.T. Kim, Development of a unique plasma burner system for emission reduction during cold start of diesel engines, SAE Tech. Pap. 1 (2014), https://doi.org/10.4271/2014-01-1490.
[49] D.K. Dinh, H.S. Kang, S. Jo, D.H. Lee, Y.-H. Song, Partial oxidation of diesel fuel by plasma – kinetic aspects of the reaction, Int. J. Hydrogen Energy 42 (2017) 22756–22764, https://doi.org/10.1016/j.ijhydene.2017.07.164.
[50] H.-S. Kang, D.H. Lee, K.-T. Kim, S. Jo, S. Pyun, Y.-H. Song, S. Yu, Methane to acetylene conversion by employing cost-effective low-temperature arc, Fuel Process. Technol. 148 (2016) 209–216, https://doi.org/10.1016/j.fuproc.2016.02.028.
[51] D.H. Lee, K.-T. Kim, M.S. Cha, Y.-H. Song, Optimization scheme of a rotating gliding arc reactor for partial oxidation of methane, Proc. Combust. Inst. 31 (2007) 3343–3351, https://doi.org/10.1016/j.proci.2006.07.230.
[52] D.K. Dinh, D.H. Lee, Y.-H. Song, S. Jo, K.-T. Kim, Arc length control for efficiency enhancement of energy usage in plasma dry reforming process, J. CO2 Util. 28 (2018) 274–282, https://doi.org/10.1016/j.jcou.2018.10.007.
[53] F. Zhu, X. Li, H. Zhang, A. Wu, J. Yan, M. Ni, H. Zhang, A. Buekens, Destruction of toluene by rotating gliding arc discharge, Fuel 176 (2016) 78–85, https://doi.org/10.1016/j.fuel.2016.02.065.
[54] H. Zhang, C. Du, A. Wu, Z. Bo, J. Yan, X. Li, Rotating gliding arc assisted methane decomposition in nitrogen for hydrogen production, Int. J. Hydrogen Energy 39 (2014) 12620–12635, https://doi.org/10.1016/j.ijhydene.2014.06.047.
[55] H. Zhang, F. Zhu, X. Li, K. Cen, C. Du, X. Tu, Rotating gliding arc assisted water splitting in atmospheric nitrogen, Plasma Chem. Plasma Process. 36 (2016) 813–834, https://doi.org/10.1007/s11090-016-9700-y.
[56] A. Wu, J. Yan, H. Zhang, M. Zhang, C. Du, X. Li, Study of the dry methane reforming process using a rotating gliding arc reactor, Int. J. Hydrogen Energy 39 (2014) 17656–17670, https://doi.org/10.1016/j.ijhydene.2014.08.036.
[57] J.L. Liu, H.W. Park, W.J. Chung, D.W. Park, High-efficient conversion of CO2in AC-Pulsed tornado gliding arc plasma, Plasma Chem. Plasma Process. 36 (2016) 437–449, https://doi.org/10.1007/s11090-015-9649-2.
[58] A. Gutsol, J.A. Bakken, A new vortex method of plasma insulation and explanation of the Ranque effect, J. Phys. D Appl. Phys. 31 (1998) 704–711, https://doi.org/10.1088/0022-3727/31/6/018.
[59] M. Ramakers, J.A. Medrano, G. Trenchev, F. Gallucci, A. Bogaerts, Revealing the arc dynamics in a gliding arc plasmatron: a better insight to improve CO2 conversion, Plasma Sources Sci. Technol. 26 (2017) 125002, https://doi.org/10.1088/1361-6595/aa9531.
[60] G. Trenchev, S. Kolev, W. Wang, M. Ramakers, A. Bogaerts, CO2 conversion in a gliding Arc plasmatron: multidimensional modeling for improved efficiency, J. Phys. Chem. C 121 (2017) 24470–24479, https://doi.org/10.1021/acs.jpcc.7b08511.
[61] G. Trenchev, A. Bogaerts, Dual-vortex plasmatron: a novel plasma source for CO2 conversion, J. CO2 Util. 39 (2020) 101152, https://doi.org/10.1016/j.jcou.2020.03.002.
[62] S. Gangoli, A. Gutsol, A. Fridman, Rotating non-equilibrium gliding arc plasma disc for enhancement in ignition and combustion of hydrocarbon fuels, Mech. Eng. (2014).
[63] J. Gonzalez-Aguilar, G. Petitpas, A. Lebouvier, J.D. Rollier, A. Darmon, L. Fulcheri, Three stages modeling of n-octane reforming assisted by a nonthermal arc discharge, Energy Fuels 23 (2009) 4931–4936, https://doi.org/10.1021/ef900475x.
[64] H. Zhang, X. Li, F. Zhu, Z. Bo, K. Cen, X. Tu, Non-oxidative decomposition of methanol into hydrogen in a rotating gliding arc plasma reactor, Int. J. Hydrogen Energy 40 (2015) 15901–15912, https://doi.org/10.1016/j.ijhydene.2015.09.052.
[65] A.E. Lutz, R.W. Bradshaw, L. Bromberg, A. Rabinovich, Thermodynamic analysis of hydrogen production by partial oxidation reforming, Int. J. Hydrogen Energy 29 (2004) 809–816, https://doi.org/10.1016/j.ijhydene.2003.09.015.
[66] D.H. Lee, K.T. Kim, M.S. Cha, Y.H. Song, Effect of excess oxygen in plasma reforming of diesel fuel, Int. J. Hydrogen Energy 35 (2010) 4668–4675, https://doi.org/10.1016/j.ijhydene.2010.02.091.
[67] M.J. Gallagher, R. Geiger, A. Polevich, A. Rabinovich, A. Gutsol, A. Fridman, On-board plasma-assisted conversion of heavy hydrocarbons into synthesis gas, Fuel. 89 (2010) 1187–1192, https://doi.org/10.1016/j.fuel.2009.11.039.
[68] J.L. Liu, H.W. Park, W.J. Chung, D.W. Park, High-efficient conversion of CO2 in AC-Pulsed tornado gliding arc plasma, Plasma Chem. Plasma Process. 36 (2016) 437–449, https://doi.org/10.1007/s11090-015-9649-2.
[69] U. Bossel, Well-to-Wheel studies, heating values, and the energy conservation principle, Proc. Eur. Fuel Cell Forum. (2003) 1–5. http://www.ppwpp.org/customers/109022312245076/filemanager/Well_to_Wheel_Studies_Heating_Values_and_the_Energy_Conserva.pdf.
[70] D. Pakhare, J. Spivey, A review of dry (CO2) reforming of methane over noble metal catalysts, Chem. Soc. Rev. 43 (2014) 7813–7837, https://doi.org/10.1039/c3cs60395d.
[71] X. Tao, M. Bai, X. Li, H. Long, S. Shang, Y. Yin, X. Dai, CH4-CO2 reforming by plasma - Challenges and opportunities, Prog. Energy Combust. Sci. 37 (2011) 113–124, https://doi.org/10.1016/j.pecs.2010.05.001.
[72] W. Rodi, Comparison of LES and RANS calculations of the flow around bluff bodies, J. Wind Eng. Ind. Aerodyn. 71 (1997) 55–75.